Chinese Chemical Letters 31 (2020) 530–534

Contents lists available at ScienceDirect

Chinese Chemical Letters

journal homepage: www.elsevier.com/locate/cclet

Communication

Cobalt sulfides as efficient catalyst towards oxygen reduction reactions

Shuo Yao[a,b], Taizhong Huang[a,*], Hengyi Fang[a], Jiemei Yu[a], Mayilvel Dinesh Meganathan[a], Zhaoxin Cui[a], Xianxia Yuan[b,*]

[a] Shandong Provincial Key Laboratory of Fluorine Chemistry and Chemical Materials, School of Chemistry and Chemical Engineering, University of Jinan, Ji'nan 250022, China
[b] Department of Chemical Engineering, Shanghai Jiao Tong University, Shanghai 200240, China

ARTICLE INFO

Article history:
Received 11 March 2019
Received in revised form 25 April 2019
Accepted 29 April 2019
Available online 30 April 2019

Keywords:
Oxygen reduction reaction
Catalysts
Cobalt sulfides
Reduced graphene oxide
Catalytic performance

ABSTRACT

Developing low-cost and high performance catalysts to replace precious metal based catalysts for oxygen reduction reaction (ORR) is one of the most feasible ways to promote the commercial application of fuel cells. In this work, flower-like CoS and octahedral CoS_2 are synthesized by a facile one-pot hydrothermal method without any adjunction of surfactants or follow-up thermolysis, their catalytic performance towards ORR in alkaline electrolyte are comparatively investigated. The results reveal that CoS_2 outperforms CoS owing to the higher electron density around S—S bond of S_2^{2-} in the crystal structure, which promotes the adsorption of oxygen on catalyst surface and facilitates the breakage of O—O bond in oxygen, leading to direct 4-electron transfer ORR. When CoS_2 particles are dispersed on the surface of rGO with large surface area, their ORR performance could be further improved.

With the increasing requirement for high efficiency new energy, great efforts have been conducted to develop fuel cells owing to their advantages of non-pollutant and superior energy conversion efficiency [1–3]. Oxygen reduction reaction (ORR) is one of the major factors determining the performance of fuel cells. In general, it is expected that the ORR can proceed *via* a 4-electron process, which fully utilizes the potential of oxygen [4–6]. Pt/C is consented to be the most efficient ORR catalyst judging from its high onset potential and 4-electron-reaction pathway [7,8]. However, high cost and scarcity of Pt have inhibited large-scale commercial applications of fuel cells [9–11]. Exploring non-noble-metal based catalysts with low cost and excellent catalytic performance is a feasible way to fasten the development of fuel cells [12,13].

Fe, Co and Ni based transition metals as well as their compounds have been paid much attention as the substitute of Pt/C with superior catalytic activities [14–17]. As a typical member of them, cobalt sulfides have been widely investigated [18–20]. Cobalt and sulfur can form a variety of compounds with different stoichiometric states, such as CoS, CoS_2, Co_3S_4, Co_4S_3, Co_9S_8, $Co_{1-x}S$ [4,18], making the synthesis of a stable compound with good crystallinity rather difficult [21]. Furthermore, the accumulation and stacking of cobalt sulfides nanoparticles also inhibit the catalytic performance. Many works on CoS_2 as ORR catalysts have been reported, but the activity and durability are still dissatisfactory. For example, Jakub *et al.* [22] found the agglomeration of large CoS_2 particles reduces catalytic activity of CoS_2 as ORR catalysts. Some researches fabricated Co_2S particles with beautiful morphology, but the active sites were blocked and the activity was reduced [21]. Using conductive carbon as a support is a generally adopted strategy to enhance the performance of catalysts [23,24]. For example, Liang *et al.* [25] reported the improved ORR activity of Co_3O_4 when supported on the surface of N-doped graphene, better ORR performance of CoSe could be achieved by loading on carbon substrate [26], Cao [27] and his coworkers fabricated a Co_9S_8/nitrogen-doped carbon nanocomposites as a bifunctional catalyst and applied in oxygen reduction/evolution reactions with high catalytic activity. Reduced graphene oxide (rGO) is a typical material in carbon group, its excellent conductivity and high specific surface area makes it a potential catalyst support. When a catalyst is uniformly distributed on its surface, the conductivity as well as the catalytic performance is expected to be promoted.

Herein, both flower-like CoS and octahedral CoS_2 materials were synthesized through a facile one-pot hydrothermal method without any adjunction of surfactants or follow-up thermolysis, their catalytic performance towards ORR were comparatively investigated. Then, the rGO supported catalyst was synthesized to further improve the performance. Thus obtained CoS_2/rGO showed great promise for ORR in alkaline fuel cells.

* Corresponding authors.
E-mail addresses: chm_huangtz@ujn.edu.cn (T. Huang), yuanxx@sjtu.edu.cn (X. Yuan).

https://doi.org/10.1016/j.cclet.2019.04.069
1001-8417/

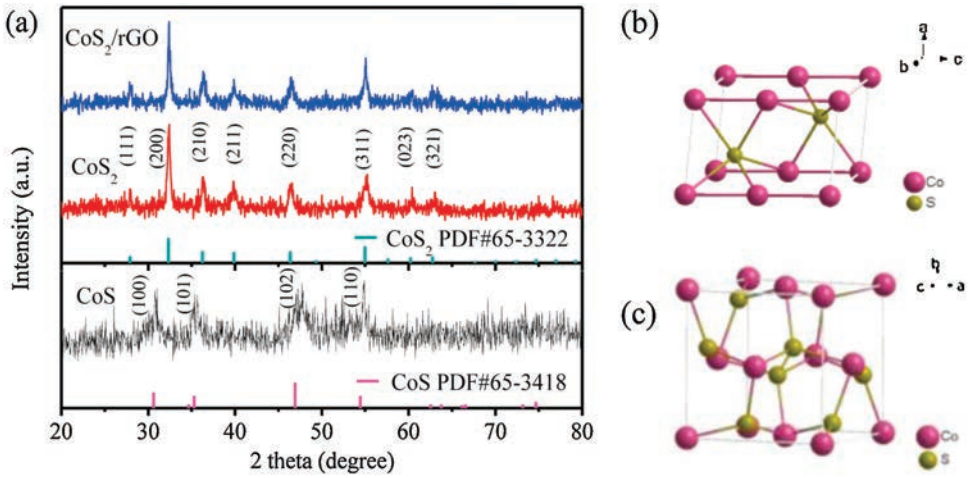

Fig. 1. XRD patterns of CoS, CoS_2 and CoS_2/rGO (a), crystal structure of CoS (b) and CoS_2 (c).

XRD patterns were captured to detect phase compositions in the as-prepared cobalt sulfides. As shown in Fig. 1a, the XRD pattern of CoS matches well with PDF card with a JCPDS No. 65-3418, implying the obtained CoS is with a hexagonal crystal structure (Fig. 1b). All the diffraction peaks of CoS_2 could be well indexed to the standard PDF #65-3322, indicating successful synthesis of CoS_2 with a cubic crystal structure (Fig. 1c). Moreover, no additional characteristic peaks could be observed in both cobalt sulfide materials, confirming the pure phase structure in the as-prepared CoS and CoS_2.

In the morphology images, the flower-like CoS particles are constituted with 2D flake-like structure unit interwoven with each other (Fig. 2a), while CoS_2 is configured with small octahedral granules (Fig. 2b). Micro-structure of the as-prepared cobalt

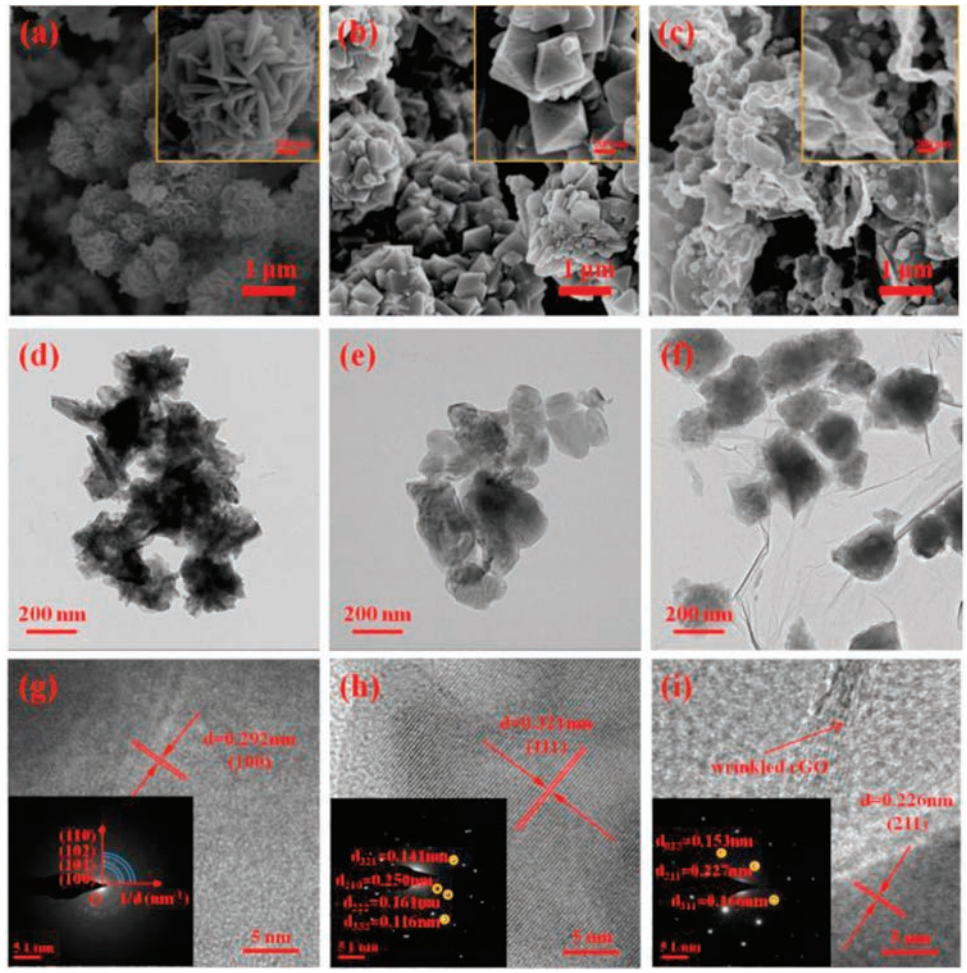

Fig. 2. SEM images of CoS (a), CoS_2 (b) and CoS_2/rGO (c); TEM images of CoS (d), CoS_2 (e) and CoS_2/rGO (f); HRTEM images of CoS (g), CoS_2 (h) and CoS_2/rGO (i), the insets in g-i are the corresponding SAED images.

sulfides was also observed with TEM, flower-like CoS assembled with flake-like unit (Fig. 2d) and octahedral CoS_2 (Fig. 2e) are clearly displayed, agreeing well with the SEM images. In the HRTEM images, the d-spacing of 0.292 nm for CoS (Fig. 2g) matches the (100) facet of hexagonal CoS (PDF #65-3418), while the spacing of 0.321 nm (Fig. 2h) is corresponding to (111) facet of cubic CoS_2 (PDF #65-3322). Moreover, the SAED patterns inserted in Figs. 2g and h were also employed to have a deeper insight into the crystallographic structure of the as-prepared cobalt sulfides. The concentric rings for CoS could be assigned to the (100), (101), (102) and (110) planes of hexagonal CoS (PDF #65-3418), and the spots for CoS_2 agree with the (332), (222), (210) and (321) facets of cubic CoS_2 (PDF #65-3322).

Electrochemical performance of CoS and CoS_2 were comparatively investigated in oxygen-saturated 0.1 mol/L KOH solution. In CV curves shown Fig. 3a, the obvious peaks in the cathodic direction imply both CoS and CoS_2 are capable of catalyzing ORR, but careful comparison reveals higher peak potential and higher peak current density of CoS_2 than CoS, indicating better catalytic performance of CoS_2. Linear sweeping voltammetry (LSV) curves for both materials were recorded with RDE at a rotating rate of 1600 rpm and the results are displayed as Fig. 3b. In the whole studied potential range, CoS_2 delivers evidently higher current density than CoS, it also demonstrates clearly higher ORR onset potential and the half-wave potential. The lower Tafel slope in Fig. 3c confirms again the superior performance of CoS_2.

To understand the different catalytic performance of CoS_2 and CoS towards ORR, RDE and RRDE experiments were conducted. Figs. 4a and c depicts the RDE curves of both materials in O_2-saturated 0.1 mol/L KOH electrolyte at various electrode rotating speeds from 900 rpm to 2025 rpm. For each catalyst, the current density increases with the increase in electrode rotating rate, owing to the enhanced oxygen diffusion [28]. Generally, the electron transfer number (n) during ORR can be calculated with RDE data and K-L plot according to equations described in Supporting information [29]. When J^{-1} is plotted against $\omega^{-1/2}$, slope of the obtained line could be used to calculate the value of n. Thus obtained K–L plots are displayed in Figs. 4b and d using the current densities at 0.45, 0.50, 0.55 and 0.60 V, respectively, in the RDE data. The calculated n values for of CoS and CoS_2 are 3.5 and 3.9, respectively, meaning that the ORR catalyzed by CoS_2 is almost through a 4-electron transfer pathway, while the reaction by CoS proceeds by parallel 4-electron and 2-electron processes [11]. These results declare CoS_2 has faster ORR kinetics than CoS.

The catalytic mechanism of CoS and CoS_2 for ORR was also investigated with RRDE and the results are shown in Fig. S2a (Supporting information). With these data, the value of n and the H_2O_2 yield (H_2O_2%) could be calculated using the equations of 3 and 4 displayed in Supporting information [30]. The obtained potential dependence of n and H_2O_2% is displayed as Fig. S2b (Supporting information). Similar to the results above from RDE, the electron-transfer number of CoS_2 is clearly larger than that of CoS, while its H_2O_2 yield is evidently smaller by about 10%, verifying again the superior performance of cobalt disulfide including higher ORR activity and faster kinetics. This is probably due to the fact that the higher electron density around S—S bond of S_2^{2-} in CoS_2 crystal structure than that around S^{2-} in CoS promotes the adsorption of oxygen on the catalyst surface and facilitates the breakage of O—O bond in oxygen leading to direct 4-electron transfer ORR [31,32].

In order to further improve the ORR performance of CoS_2, rGO with high specific surface area and good conductivity was employed to form the composite of rGO supported CoS_2 (CoS_2/rGO) as catalyst, its XRD pattern is also shown in Fig. 2a along with that of CoS_2 and CoS for comparison. The characteristic peaks closely match that of bare CoS_2, proving the existence and successful synthesis of CoS_2 in this composite. The absence of peaks for rGO is probably because of the thin layers [25]. In the SEM image displayed as Fig. 2c, wrinkled rGO can be clearly observed with uniformly dispersed CoS_2 particles on its surface, confirming the existence of rGO. Moreover, the size of CoS_2 particles in CoS_2/rGO is greatly smaller than that of the bare CoS_2, it is only one

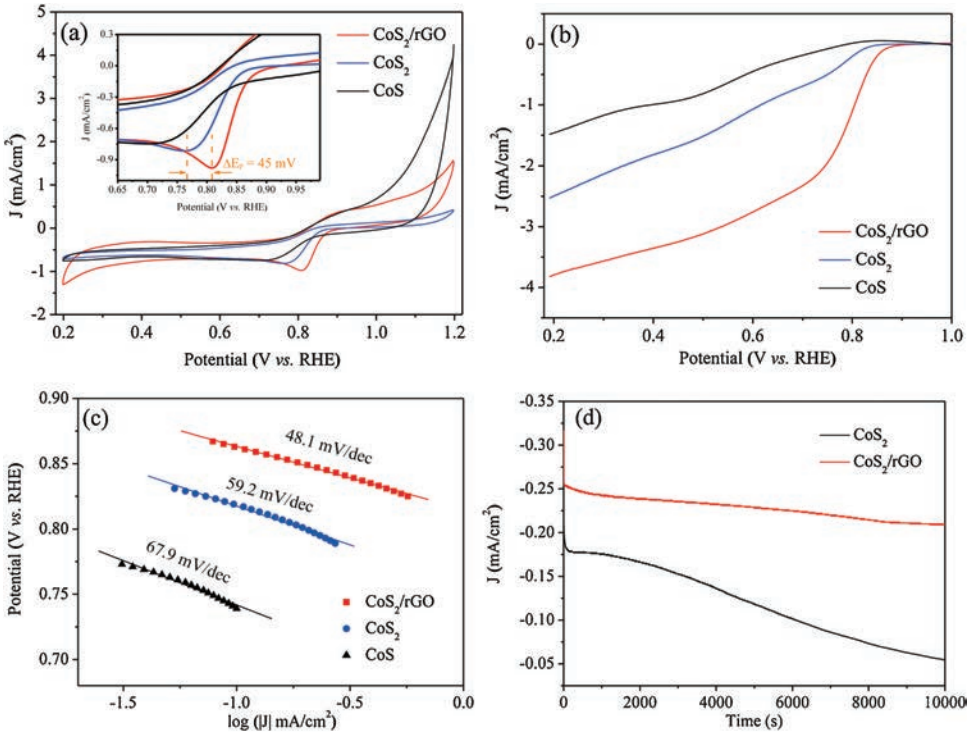

Fig. 3. CV curves (a) of CoS, CoS_2 and CoS_2/rGO in O_2-saturated 0.1 mol/L KOH electrolyte at a potential sweeping rate of 5 mV/s, RDE curves (b) of CoS, CoS_2 and CoS_2/rGO in O_2-saturated 0.1 mol/L KOH electrolyte at 1600 rpm at a sweeping rate of 5 mV/s, Tafel plots (c) of CoS, CoS_2 and CoS_2/rGO, long-term stability tests (d) of CoS_2 and CoS_2/rGO.

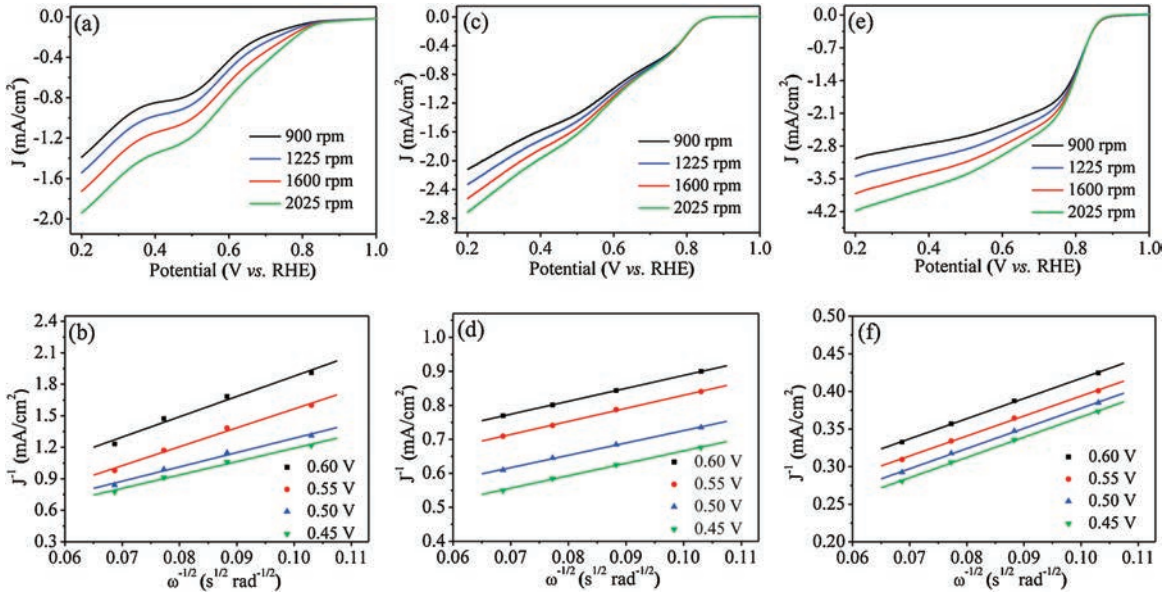

Fig. 4. RDE curves of CoS (a), CoS_2 (c) and CoS_2/rGO (e) in O_2-saturated 0.1 mol/L KOH electrolyte at a potential sweeping rate of 5 mV/s and various electrode rotating rates, and the corresponding K-L plots of CoS (b), CoS_2 (d) and CoS_2/rGO (f) at various potentials.

fourth or less of the latter. This could be attributed to the influence of rGO according to Chang *et al.* [33] and Wang *et al.* [29], probably because of the interactions between rGO and cobalt sulfides and also the large surface area of rGO hinders the agglomration of CoS_2 particles. The TEM images shown in Figs. 2f and i also confirm the co-existence of CoS_2 and rGO in this composite. In Fig. 2f, both the wrinkled rGO and the smaller CoS_2 particles are evidently observed. In the HRTEM image (Fig. 2i), the irregular-sized crystalline lattice fringes can be assigned to wrinkled rGO support, while the d-spacing of 0.226 nm is corresponding to (211) facet of CoS_2. The inset of SEAD pattern also demonstrates obvious diffraction spot array that could be indexed to (211), (311) and (023) facets in CoS_2.

The electrochemical performance of CoS_2/rGO was evaluated and compared with bare CoS_2. In the CV curves shown in Fig. 3a, the ORR peak potential of CoS_2/rGO is increased by 45 mV from that of CoS_2. The peak current density is also higher by about 200 mA/cm^2. In the LSV curves shown in Fig. 3b, CoS_2/rGO delivers apparently higher onset potential and strongly larger current density in the whole studied voltage range, indicating the increase of catalytic active area due to decrease of particle size. Its onset potential of 0.93 V is also higher than the reported values for similar rGO supported catalysts of $NiCo_2S_4$@N/S-rGO (0.86 V), Co_3S_4@N/S-rGO (0.85 V) and $Co_{1-x}S$/rGO (0.87 V) in 0.1 mol/L KOH electrolyte [34,35]. Meanwhile, it can be observed that the half-wave potential of CoS_2/rGO is also higher than that of bare CoS_2, demonstrating the strong synergistic effect between CoS_2 and rGO as support and the improved ORR activity of CoS_2/rGO. The decreased Tafel slope in Fig. 3c further confirms the enhanced ORR performance of CoS_2/rGO from bare CoS_2. The durability of CoS_2/rGO was evaluated with chronoamperometric measurement and compared with that of CoS_2. The current density of CoS_2/rGO reaches stable much earlier than CoS_2 as displayed in Fig. 3d, and its current density is greatly higher than CoS_2 during the whole continuous working for 10,000 s, indicating a better long-term stability as ORR catalyst. RDE and RRDE were also employed to understand the ORR performance improvement. In Figs. 4e and f, the current density of CoS_2/rGO at each rotating rate is greatly larger than that of CoS_2, and its linearity of K-L plot is evidently better than bare CoS_2, indicating first-order reaction kinetics towards the concentration of dissolved oxygen and the more similar electron transfer number per oxygen molecule within the studied potential range [36,37]. The calculated higher electron transfer number of nearly four also implies faster electron transport rate between electrode and electrolyte and higher efficiency for oxygen reduction to OH^- by accepting four electrons [38]. In the RRDE data shown in Fig. S2, CoS_2/rGO demonstrates evidently increased onset potential than the bare CoS_2, its current density on the disk electrode is greatly increased while that on the ring electrode is decreased. In Fig. S2b which displays the calculated electron transfer number and H_2O_2 yield as a function of potential, CoS_2/rGO exhibits again clearly larger n and lower H_2O_2%. These results disclose that dispersing CoS_2 on the surface of rGO as support can efficiently enhance the ORR kinetics, promote the catalytic activity and facilitate ORR to happen through 4-electron reaction pathway, resulting in enlarged ORR performance. This improvement could be attributed to two aspects. The first one is the excellent synergistic effect between CoS_2 and rGO as support, similar effects were also observed during the research on MoS_2/gaphene hybrid, which exhibited higher catalytic performance than pure MoS_2 for ORR [7,39]. Moreover, rGO with large specific surface area can improve the dispersion of CoS_2 to expose more catalytic active sites.

In this work, both flower-like CoS and octahedral CoS_2 have been successfully synthesized through a facile one-pot hydrothermal method without any adjunction of surfactants or follow-up thermolysis. Comparative study disclosed that the as-prepared CoS_2 has superior performance to CoS when employed as catalyst for ORR in alkaline electrolyte, judging from the onset potential, peak potential, half-wave potential, peak current density, Tafel slope as well as the electron transfer number and H_2O_2 yield. When supported on the surface of rGO, the particle size of CoS_2 decreased to one fourth or less of the bare CoS_2, its specific surface area is greatly enlarged and much more active sites towards ORR could be exposed, leading to enhanced ORR kinetics as well as activity.

Acknowledgments

This project was financially supported National Natural Science Foundation of China (No. 21476138), Shandong Provincial Natural Science Foundation (No. ZR2018MB036), Science Development Project of Shandong Province (Nos. 2017GGX40115 and

2016GGX102038), Project of Shandong Province Higher Educational Science and Technology Program (Nos. J17KA094, J13LD08).

Appendix A. Supplementary data

Supplementary material related to this article can be found, in the online version, at doi:https://doi.org/10.1016/j.cclet.2019.04.069.

References

[1] I.A. Khan, Y. Qian, A. Badshah, et al., ACS Appl. Mater. Interfaces 8 (2016) 17268–17275.
[2] S.G. Peera, A. Sahu, A. Arunchander, et al., Carbon 93 (2015) 130–142.
[3] M. Seredych, E. Rodriguez-Castellon, T.J. Bandosz, J. Mater. Chem. A 2 (2014) 20164–20176.
[4] Y. Gu, Y. Xu, Y. Wang, ACS Appl. Mater. Interfaces 5 (2013) 801–806.
[5] B.C.H. Steele, A. Heinzel, Nature 414 (2001) 345–352.
[6] B. Wang, X. Cui, J. Huang, et al., Chin. Chem. Lett. 29 (2018) 1757–1767.
[7] K. Zhao, W. Gu, L. Zhao, et al., Electrochim. Acta 169 (2015) 142–149.
[8] M.D. Meganathan, S. Mao, T. Huang, G. Sun, J. Mater. Chem. A 5 (2017) 2972–2980.
[9] J.P. Paraknowitsch, A. Thomas, Energy Environ. Sci. 6 (2013) 2839–2855.
[10] J. Snyder, T. Fujita, M. Chen, J. Erlebacher, Nat. Mater. 9 (2010) 904–907.
[11] K. Gong, F. Du, Z. Xia, et al., Science 323 (2009) 760–764.
[12] N. Bhandary, S. Basu, P.P. Ingole, Electrochim. Acta 212 (2016) 122–129.
[13] H. Cui, Z. Zhou, D. Jia, Mater. Horiz. 4 (2017) 7–19.
[14] Y. Hou, Z. Wen, S. Cui, et al., Adv. Funct. Mater. 25 (2015) 872–882.
[15] X.X. Wang, D.A. Cullen, Y.T. Pan, et al., Adv. Mater. 30 (2018) 1706758.
[16] S. Kumar, A. Jena, Y.C. Hu, et al., Chemelectrochem 5 (2018) 29–35.
[17] L. Hu, F. Yu, H. Yuan, et al., Chin. Chem. Lett. 30 (2019) 624–629.
[18] Y. Wang, J. Wu, Y. Tang, et al., ACS Appl. Mater. Interfaces 4 (2012) 4246–4250.
[19] N. Kumar, N. Raman, A. Sundaresan, Z. Anorg. Allg. Chem. 640 (2014) 1069–1074.
[20] B. Hu, Z. Jing, J. Fan, et al., Catal. Today 263 (2016) 128–135.
[21] D.C. Higgins, F.M. Hassan, M.H. Seo, et al., J. Mater. Chem. A 3 (2015) 6340–6350.
[22] J.S. Jirkovský, A. Bjoerling, E. Ahlberg, J. Phys. Chem. C 116 (2012) 24436.
[23] R.J. Wu, M. Liu, Y.W. Peng, et al., Chin. Chem. Lett. 30 (2019) 989–994.
[24] X. Chen, X. Zhen, H. Gong, et al., Chin. Chem. Lett. 30 (2019) 681–685.
[25] Y. Liang, Y. Li, H. Wang, et al., Nat. Mater. 10 (2011) 780–786.
[26] P. Nekooi, R. Ahmadi, M.K. Amini, J. Iran. Chem. Soc. 9 (2012) 715–722.
[27] X. Cao, X. Zheng, J. Tian, et al., Electrochim. Acta 191 (2016) 776–783.
[28] H.R. Byon, J. Suntivich, Y. Shao-Horn, Chem. Mater. 23 (2011) 3421–3428.
[29] T. Huang, S. Mao, M. Qiu, et al., Electrochim. Acta 222 (2016) 481–487.
[30] W. Gu, L. Hu, W. Hong, et al., Chem. Sci. 7 (2016) 4167–4173.
[31] I.V. Malakhov, S.G. Nikitenko, E.R. Savinova, et al., J. Phys. Chem. B 106 (2002) 1670–1676.
[32] R.A. Sidik, A.B. Anderson, N.P. Subramanian, et al., J. Phys. Chem. B 110 (2006) 1787–1793.
[33] K. Chang, W. Chen, ACS Nano 5 (2011) 4720–4728.
[34] Q. Liu, J. Jin, J. Zhang, ACS Appl. Mater. Interfaces 5 (2013) 5002–5008.
[35] W. Hailiang, L. Yongye, L. Yanguang, D. Hongjie, Angew. Chem. Int. Ed. 123 (2011) 11161–11164.
[36] M. Shen, C. Ruan, Y. Chen, et al., ACS Appl. Mater. Interfaces 7 (2015) 1207–1218.
[37] W. Li, Y. Li, H. Wang, et al., Electrochim. Acta 265 (2018) 32–40.
[38] Y. Dong, Y. Deng, J. Zeng, et al., J. Mater. Chem. A 5 (2017) 5829–5837.
[39] T. Huang, S. Mao, G. Zhou, et al., Nanoscale 6 (2014) 9608–9613.